J. Fluid Mech. (1997), *vol.* 338, *pp.* 203–230

The effect of the structure of swept-shock-wave/turbulent-boundary-layer interactions on turbulence modelling

By ARGYRIS G. PANARAS†

DLR, Institute for Fluid Mechanics, Bunsenstrasse 10, D-37073 Göttingen, Germany

(Received 9 April 1996 and in revised form 22 November 1996)

The physical reasons for the difficulty in predicting accurately strong swept-shock-wave/turbulent-boundary-layer interactions are investigated. A well-documented sharp-fin/plate flow has been selected as the main test case for analysis. The selected flow is calculated by applying a version of the Baldwin–Lomax turbulence model, which is known to provide reliable results in flows characterized by the appearance of crossflow vortices. After the validation of the results, by comparison with appropriate experimental data, the test case flow is studied by means of stream surfaces which start at the inflow plane, within the undisturbed boundary layer, and which are initially parallel to the plate. Each of these surfaces has been represented by a number of streamlines. Calculation of the spatial evolution of some selected stream surfaces revealed that the inner layers of the undisturbed boundary layer, which are composed of turbulent air, wind around the core of the vortex. However, the outer layers, which are composed of low-turbulence air, fold over the vortex and at the reattachment region penetrate into the separation bubble forming a low-turbulence tongue, which lies along the plate, underneath the vortex. The conical vortex at its initial stage of development is completely composed of turbulent air, but gradually, as it grows linearly in the flow direction, the low-turbulence tongue is formed. Also the tongue grows in the flow direction and penetrates further into the separation region. When it reaches the expansion region inboard of the primary vortex, the secondary vortex starts to be formed at its tip. Examination of additional test cases indicated that the turbulence level of the elongated tongue decreases if the interaction strength increases. The existence of the low-turbulence tongue in strong swept-shock-wave/turbulent-boundary-layer interactions creates a mixed-type separation bubble: turbulent in the region of the separation line and almost laminar between the secondary vortex and the reattachment line. This type of separation cannot be simulated accurately with the currently used algebraic turbulence models, because the basic relations of these models are based on the physics of two-dimensional flows, whereas in a separation bubble the whole recirculation region is turbulent. For improving the accuracy of the existing algebraic turbulence models in predicting swept-shock-wave/turbulent-boundary-layer interactions, it is necessary to develop new equations for the calculation of the eddy viscosity in the separation region, which will consider the mixed-flow character of the conical vortex.

---

† Present address: PO Box 64053, Athens 15710, Greece.

1. Introduction

The interaction of a swept shock wave with a boundary layer appears in those regions of a high-speed vehicle in which two surfaces intersect. Simple configurations are studied which resemble these regions. In the case of a turbulent boundary layer, the simplest and most studied configuration consists of a sharp fin (or wedge) attached normally to a flat plate at a certain distance behind its leading edge. The oblique shock wave generated by the fin interacts with the boundary layer on the plate and, as a result, the increase in pressure through the shock is smeared out on the plate and a disturbed flow pattern is observed for a considerable distance both upstream and downstream of the shock position predicted for inviscid flow. If the shock is strong enough to cause the boundary layer to separate, the topology of the flow changes significantly. Peak heating and high values of pressure have been measured in the region of intersection of the two surfaces. Early oil-flow visualizations have revealed the existence on the plate, below the separation bubble, of a separation and a reattachment line, which are straight away from the apex of the configuration and intersect upstream of it. The trace of the inviscid shock also comes from this intersection. The first flow model of the sharp-fin/plate configuration was proposed in 1974 by Token. In order to explain the high heat-transfer peak measured on the flat plate, near the root of the fin, he suggested that a conical vortex appears between the separation and the reattachment lines, which carries to its reattachment region high-energy air, from the external flow. Almost twenty years of research were required to prove this early hypothesis. Today it is known that the flow is quasi-conical. The major features of the flow field, like the shock structure and the shape of the conical vortex have been visualized, experimentally and computationally.

Though the numerical simulations of flows about sharp-fin/plate configurations have considerably contributed to the verification of the early hypotheses regarding the structure of these flows, the accuracy of the predictions is still not very satisfactory. The capability of numerical simulation of three-dimensional shock-wave/turbulent-boundary-layer interactions has been assessed by Knight (1993), who, for that purpose, examined five specific configurations (sharp fin, blunt fin, cylinder/flare, swept compression corner and crossing shocks) at Mach numbers from 2 to 8. Knight (1993) concluded that the Pitot pressure, yaw angle and surface pressure are predictable with reasonable accuracy using algebraic or two-equation turbulence models, however the surface heat transfer is not accurately predicted in strong interactions. In the particular case of the sharp-fin/plate configuration, Kim *et al.* (1991) have performed a joint experimental and computational study of skin friction in weak-to-strong interactions at Mach number 3 and 4. In their Navier–Stokes calculations they tested the most widely used turbulence models, i.e. the algebraic ones of Cebeci & Smith (1974) and of Baldwin & Lomax (1978) and the two-equation $k-\epsilon$ model, integrated to the wall or employing the wall-function technique. They found that their computations agree well with the data for moderate interaction strenghs, but systematically underpredict the data with increasing interaction strength. Also, the secondary separation line which, according to the experimental data, exists in the surface flow pattern has not been predicted in their calculations. It is worth noting that according to the sharp-fin/plate results of Knight *et al.* (1987), who also applied algebraic and two-equation turbulence models, the flowfield predictions of the two models are similar though they provide eddy viscosities which differ by as much as a factor of 14 (the smaller values are given by the $k-\epsilon$ model).

The type of crossflow separation which is established at strong interactions about a sharp-fin/plate configuration is also observed in flows about slender bodies at high

incidence. Crossflow separation occurs when fluid flowing circumferentially from the windward to the leeward side of such a body separates from the sides of the body along a separation line roughly parallel to its longitudinal axis. The fluid rolls up and forms two primary vortices on the leeward side, on both sides of the symmetry plane. The extent of the crossflow and the strength of the vortices grow as the angle of attack is increased. If the strength of the primary vortices is sufficiently large, secondary separation is induced below the primary ones. Application of the two-layer turbulence model of Baldwin & Lomax (1978) to flows about slender bodies at high incidence results in underestimation of the size of the primary vortices and non-appearance of the secondary ones (see Degani & Schiff 1986 and Panaras & Steger 1988), i.e. conditions which exist also in the simulation results of the sharp-fin/plate configuration. Degani & Schiff (1986) have attributed these conditions to large values of the estimated eddy-viscosity coefficient in the separated region, due to the involvement in the calculation procedure of the primary vortices which overlay the boundary layer. If the contribution of the vortices is disregarded when the eddy-viscosity coefficient is estimated, then, as Degani & Schiff (1986) have demonstrated, the agreement with the experimental data is better and the secondary separation lines appear in the calculated pattern of the skin-friction lines. These authors have developed an appropriate computation procedure, which excludes the primary vortices from the calculation of the eddy viscosity, by considering the first (lower) maximum of the profiles of the moment of vorticity of the viscous layers and not the second (or higher) one. The first maximum corresponds to the boundary layer, and the second one to the overlying primary vortex. Details will be given in § 3.2.

Panaras & Steger (1988) have developed an alternative numerical procedure for implementing an algorithm of Degani–Schiff type in an application of the Baldwin–Lomax turbulence model. This procedure is useful for a complex flow structure, where the profiles of the moment of vorticity of the boundary layer exhibit more than two maxima. More recently Panaras & Stanewsky (1992), noting the similarity of the topology of the flow structure between a sharp-fin/plate configuration and a slender body at high incidence, have applied the Panaras & Steger (1988) numerical procedure to the calculation of one of the flows studied at the Pennsylvania State University (Kim *et al.* 1991). They have found that the resulting solution agrees very well with the experimental data of G. Settles and his associates (wall pressure, skin friction, surface flow angle). Also, post-processing of the solution revealed the existence of a weak secondary vortex. Application of the standard Baldwin–Lomax model resulted in poor results, similar to those reported previously by Kim *et al.* (1991).

In the present paper the structure of the separation vortex in a strong swept-shock-wave/turbulent-boundary-layer interaction is studied, for the purpose of explaining why the algebraic and the $k-\epsilon$ turbulence models fail to predict accurately this type of flow. One of the sharp-fin/plate flows examined by Kim *et al.* (1991) is used as a model. The selected flow is simulated by application of the turbulence modelling procedure of Panaras & Steger (1988) in a upwind Navier–Stokes solver. After the validation of the results, by comparison with the related experimental data, the flow field is analysed by an appropriate visualization technique. It is shown that the outer layers of the undisturbed boundary layer, which are composed of low-turbulence air, fold over the conical vortex and at the reattachment region penetrate into the separation bubble and form a low-turbulence tongue, which lies along the plate, underneath the vortex. The effect of this low-turbulence tongue on turbulence modelling is discussed. Also, the remarkable accuracy of calculations which are based on the concept introduced by Degani & Schiff (1986) is explained.

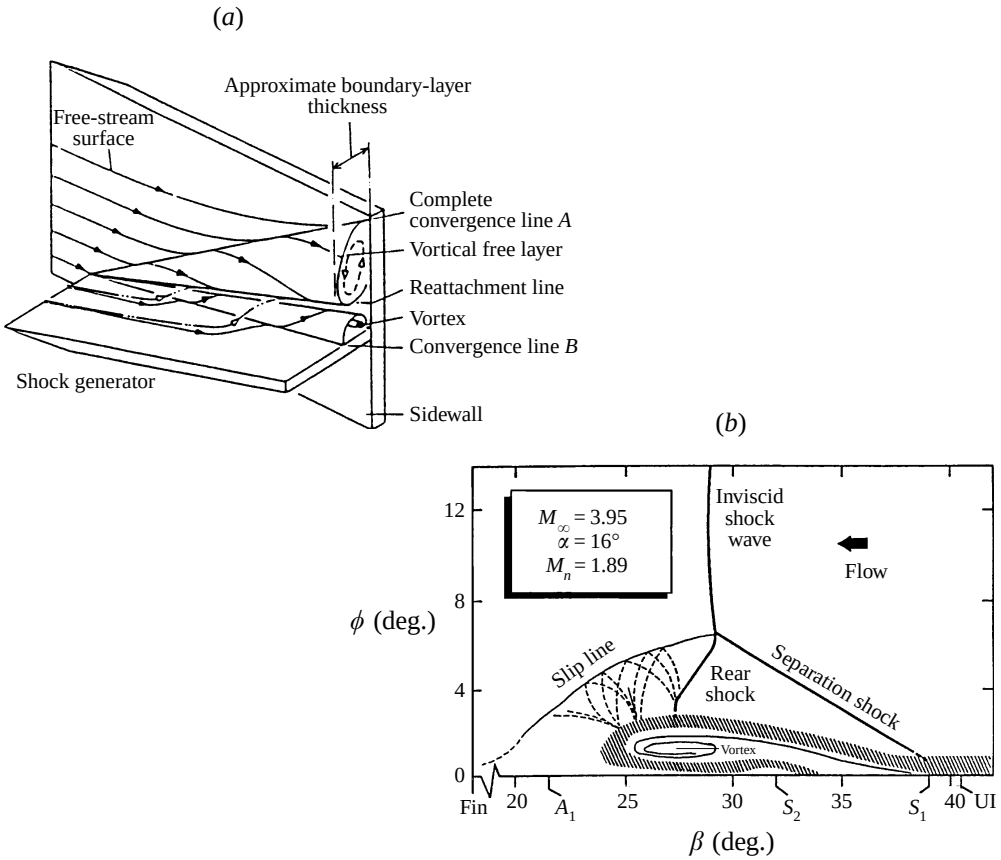

FIGURE 1. Flow field models: (*a*) proposed by Kubota & Stollery (1982); (*b*) proposed by Alvi & Settles (1992).

2. Brief review of the physics of the flow about a sharp fin/plate

In this section a brief review of the physics of the flow about a sharp-fin/plate configuration will be presented. The experimental and the computational aspects of this type of flow are discussed in the reviews of Settles (1993) and Knight (1993), respectively. In a more recent review the present author (Panaras 1996) examines in addition the axial corner (two wedges attached normally), since close to its surfaces the flow is similar to that observed about a sharp-fin/plate configuration.

The first major improvement in the modelling of the flow about a sharp-fin/plate configuration occurred in 1982 when Kubota & Stollery, based on their own experimental results, improved the flow model proposed by Token (1974). For strong interactions Kubota & Stollery (1982) proposed the flow model shown in figure 1(*a*). The separated flow in their model is characterized by two counter-rotating vortices, a tight vigorous roughly circular one in the corner with a weak very elongated one above it. In addition to the separation vortices, these authors also investigated the structure of the shock system. According to their vapour-screen pictures, when the angle of the fin is larger than that required for the appearance of separation there is evidence of shock splitting into a λ-shape near the edge of the boundary layer.

During the eighties, significant progress in the investigation of the physics of the sharp-fin/plate flows was made in USA at the Universities of Princeton, Penn State and

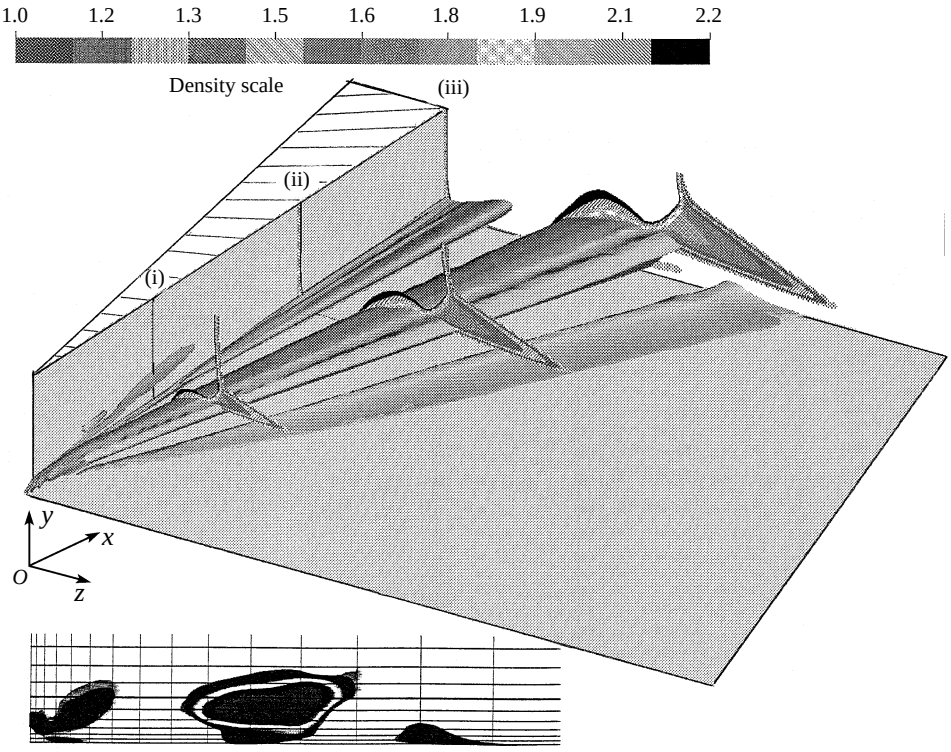

FIGURE 2. Perspective view of the conical vortices and of the shock waves (Panaras 1992).

Rutgers (S. Bogdonoff, G. Settles, D. Knight and their associates) and at NASA/Ames (C. Horstman). In their combined experimental and computational works they have studied in detail the topology of the surface flow pattern and various scaling laws. Also, they have demonstrated numerically that the trajectories of streamlines which originate upstream of the separation line are lifted off the wall, cross the separation line and rotate in the direction in which the separation vortex should rotate. More recently the USA group has presented cuts of the flow field normal to the shock in a sharp-fin/plate configuration using the non-intrusive planar laser scattering (PLS) technique (Alvi & Settles 1992), or refined calculations (Knight *et al.* 1992). These cuts visualize very clearly the λ-shock structure and the shape of the cross-section of the separation vortex. Also, Alvi & Settles (1992) combined the PLS results with previous wall-pressure and skin-friction measurements to construct a physical flow-field model. An example is shown in figure 1(*b*) for a $M_\infty = 4.0$, $\alpha = 16^\circ$ flow. As coordinates the conical angles β (horizontal) and ϕ (vertical) are used. These angles are measured from the fin leading edge with respect to the free-stream direction. Symbol A_1 denotes the position of the reattachment line, S_1 and S_2 the primary and secondary separation lines, respectively.

The conical flattened separation vortex and the smaller vortex in the corner region (postulated by Kubota & Stollery 1982), have been visualized in space numerically by the present author, who in addition studied quantitatively the quasi-conical nature of the flow (Panaras 1992). Figure 2, taken from that paper, includes all the critical elements of the swept-shock-wake/turbulent-boundary-layer interaction. The

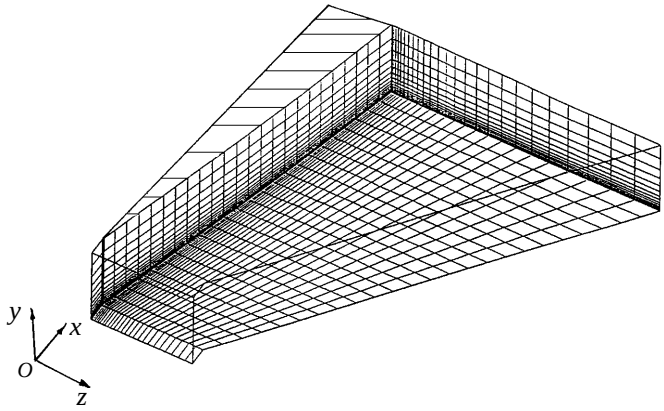

FIGURE 3. Computational grid.

vortices which are expected to appear in this type of flow are visualized in the three-dimensional space by the contours of the eigenvalues of the velocity gradient field (Vollmers, Kreplin & Meier 1983). It is observed that, as expected, the flow is dominated by a large vortical structure, which lies on the flat plate and whose core has a remarkable conical shape with a flattened elliptical cross-section. Also on the flat plate, on the side of the main vortex, a thin vortex has developed in the direction of the flow. This is not an independent vortex, but the core of the boundary layer which lifts off the surface, along the separation line, and rolls up to form the conical vortex. Along the vertical fin and close to the corner, the longitudinal vortex, mentioned by Kubota & Stollery (1982), is seen. It also develops quasi-conically, but with a smaller rate of increase, compared to the primary conical vortex structure. The density contours at three cross-sections of the flow, which are also displayed in figure 2, visualize the shock system which is formed along and on top of the conical vortex.

3. Description of the numerical procedure

3.1. *Numerical method, boundary conditions*

The Reynolds-averaged Navier–Stokes equations, with the x-derivative (streamwise direction) of the viscous terms ignored, are solved at the interior grid points of the mesh shown in figure 3. The inviscid and the viscous fluxes are treated implicitly. A second-order central differencing is applied to the viscous fluxes. The inviscid fluxes are determined by the upwind total variation diminishing (TVD) scheme of Yee & Harten (1987), which uses Roe's approximate Riemann solver (Roe 1981) and Harten's second-order modified flux approach. Alternating Gauss–Seidel relaxation in the streamwise direction is employed.

Owing to the simplicity of the geometry of the fin–plate configuration, the mesh shown in figure 3 was generated algebraically (for clarity each third or fourth grid line is shown). A clustering was applied close to the plate and to the fin, for an adequate resolution of the viscous effects. In each crossflow-direction plane (z-, y-directions) 105×111 points are used, while in the streamwise x-direction there are 77 grid planes uniformly spaced, with $\Delta x = 0.5\delta_o$, where δ_o is the thickness of the boundary layer at the start of calculation. The inflow plane is located at a distance equal to $2\delta_o$ upstream of the leading edge of the fin, and the downstream boundary at $x = 36.5\delta_o$.

The height of the computational field is $9.23\delta_o$. The width is uniform before the fin, equal to $10.9\delta_o$, but from there on it increases to $z = 29.4\delta_o$ at the outflow plane.

The mesh is very fine (897,435 points), especially in the direction normal to the plate. More particularly, 69 points are used for the simulation of the undisturbed boundary layer, while the minimum value of y^+ at the first point off the plate is 0.15 and its maximum value equal to 0.5. The minimum number of subsonic points is 11. Initially, 95 points in the y-direction and minimum $y^+ = 0.5$ were used. For these values the level of the skin friction upstream of the interaction was too high. An increase of the number of points to 111 and a reduction of the minimum y^+ to 0.15 resulted in a stable solution which did not change when the minimum y^+ was further decreased to 0.075.

The boundary-layer profile upstream of the interaction region is used as the boundary condition on the inflow plane, as well as the initial condition of the flow field. This profile was calculated by a two-dimensional procedure, from the leading edge of the flat plate to the edge of the fin. The profile was very close to the experimental one. Furthermore, the thickness of the undisturbed boundary layer, δ_o, is the length scale of the interaction. The gradients of the flow parameters are set equal to zero, on the far-field (upper and lateral boundaries) and on the outflow boundary. The walls are assumed impermeable and no-slip boundary conditions are applied. The pressure gradient normal to the walls is taken equal to zero, as well as the temperature gradient (the walls are assumed adiabatic).

3.2. *Turbulence model*

A modified version of the two-layer Baldwin & Lomax (1978) turbulence model was applied to the numerical simulation of the sharp-fin/plate flow decribed in the present paper.

In the inner-layer Baldwin & Lomax (1978) use the Prandtl–van Driest formulation:

$$(\mu_t)_{inner} = \rho(\kappa D\eta)^2\omega \tag{3.1}$$

where κ is the von Kármán constant (equal to 0.41), D is the van Driest damping factor, ω is the absolute value of the vorticity and η is the distance normal to the wall. The damping fator is $D = 1 - \exp(-u_\tau/26\nu_w)$, where $u_\tau = (|\tau_w|/\rho_w)^{1/2}$, τ_w is the wall shear stress and ν_w the wall kinematic eddy viscosity.

In the outer region, the following equation is used:

$$(\mu_t)_{outer} = C_{cp}(0.0168\rho F_{wake}\gamma), \tag{3.2}$$

$$F_{wake} = \min\left\{ \begin{array}{l} \eta_{max}F_{max}, \\ C_{wk}\eta_{max}u_{dif}^2/F_{max}. \end{array} \right\}$$

The quantity F_{max} is the maximum value of the function $F(\eta) = \eta\omega D$, and η_{max} is the value of η at which it occurs; the Klebanoff intermittency factor γ is given by

$$\gamma = [1 + 5.5(\eta/\delta)^6]^{-1}; \tag{3.3}$$

and u_{dif} is the difference between maximum and minimum velocity in the profile. The thickness of the boundary layer is defined by $\delta = \eta_{max}/C_{Kleb}$. The constants appearing in the above relations are: $C_{cp} = 1.6$, $C_{wk} = 0.25$, $C_{Kleb} = 0.3$. In the particular geometry of the sharp-fin/plate configuration, where there are two intersecting surfaces, a 'modified distance' is used, originally proposed by Hung & MacCormack (1978) to

account for the turbulent mixing length near the intersection of the surfaces:

$$\eta = \frac{2yz}{y + z + (y^2 + z^2)^{1/2}}. \tag{3.4}$$

The values of F_{max} and η_{max} must be determined twice, once for the plate and once for the fin. Then they have to be combined at the junction of the two surfaces. This topic is analysed in detail in the work of Gerhold & Krogmann (1993), where an appropriate blending function is proposed. In the present paper the simplified approach of calculating F_{max} and η_{max} along grid lines which are normal only to the plate has been applied. Since the calculated values of the function F_{wake} with this approach are almost zero close to the fin (see figures 13 and 14), the predicted boundary layer of the fin is almost laminar. This is very close to the truth because actually the flow along the fin is laminar, at least above the edge of the undisturbed boundary layer of the plate. We feel that the double-calculation procedure is necessary only in the case of simulation of axial corners, where both surfaces start at the same axial location.

We have mentioned in the introduction that a point which needs attention when the Baldwin–Lomax model is applied to flows with substantial crossflow separation, is the proper calculation of the distance from the wall where the moment of vorticity, $F(\eta)$, takes the maximum value. Degani & Schiff (1986) have observed that while in the case of attached boundary layers the profile of $F(\eta)$ has a single maximum, in the presence of crossflow separation a second maximum, of greater value, appears. This second maximum is due to the overlying vortical structure. Thus, if in a code the computer searches outward along each normal to a surface to determine the peak of $F(\eta)$, it will select the second maximum. This will cause an underestimation of the extent of the crossflow (because μ_t will take greater values, i.e. the calculated flow will be more turbulent than the real one). Degani & Schiff (1986) modified their algorithm, so that the first peak of $F(\eta)$ is selected in each profile.

Reviewing profiles of the vorticity moment at various streamwise and circumferential stations of the flow about a prolate spheroid, Panaras & Steger (1988) observed that a boundary layer may have two peaks of the moment of vorticity, one in the sublayer and one far from the wall. Thus, a computerized search for the first maximum of the moment of vorticity may select the sublayer value and not that of the boundary layer. For this reason, they suggested an alternative procedure, according to which initially the flow is computed by using the standard Baldwin–Lomax model, then the user reviews the profiles of the moment of vorticity at various streamwise and circumferential stations and draws a single horizontal line that separates the boundary layer from the overlying vortical structure. Since the cross-flow vortices lift-off away from the body in the downstream direction it is possible, to an engineering approximation, to define this dividing line. This is easy if in the related figures the number of the index K of the grid is used as vertical coordinate instead of the physical distance from the wall y, because in this case there is a magnification of the wall region. Then a single cut-off value K_{cut} is assigned to the index K, and the search for the maximum value of the moment of vorticity is repeated between $K = 1$ and K_{cut}. With this simple technique, the overlying vortical structure is excluded from the process of calculation of the maximum values of the moment of vorticity. This second calculation converges rather fast, because only a part of the flow is affected. Then, the profiles of the vorticity moment are plotted again and checked as to whether the selected K_{cut} value is still appropriate. Panaras & Steger (1988) have found that

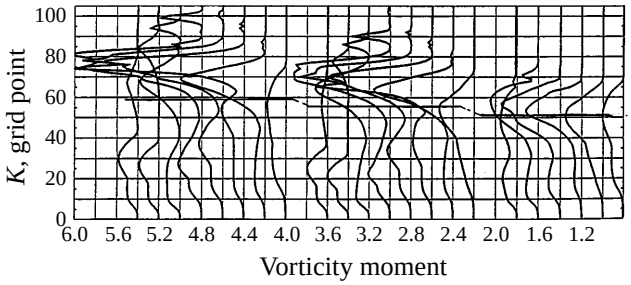

FIGURE 4. Variation of the profiles of the moment of vorticity along three cross-sections.

the K_{cut} value does not change significantly. The final calculation, with the corrected value of K_{cut}, requires for its convergence very few integration steps.

The constant-cutoff-distance technique proposed by Panaras & Steger (1988) is useful for a complex flow structure, where the profiles of the moment of vorticity of the boundary layer exhibit more than two maxima in the separation region. The flow examined here is of this category. Furthermore, Degani and Schiff in a more recent paper (Degani, Schiff & Levy 1991) discuss the problem of the critical conditions which exist near the separation line, regarding the calculation of y_{max}, since in this region the peaks merge. One of the alternatives which they propose for solving this problem is to use a constant-cutoff-distance for all rays near the separation line, based on the radial distance of the peak in $F(y)$ found on the symmetry plane of the windward side.

4. Results

The experiments performed in the Supersonic Wind Tunnel Facility of the Penn State University by G. Settles and his associates are perhaps the best available data for code validation in swept-shock-wave/turbulent-boundary-layer interactions. These tests are well documented in Settles & Dodson (1991). The measurements include skin friction and wall flow angle distribution along a circular arc at a radius $R = 88.9$ mm from the leading edge of the fin, as well as wall pressure distribution, along a circular arc at a radius $R = 101.1$ mm. The skin-friction data were produced by the recently developed laser interferometer skin friction technique. Also available is a picture of the pattern of the skin-friction lines along the plate, obtained by using a kerosene-lampblack visualization technique. The characteristic parameters of the main flow which will be simulated in this paper are: $M_\infty = 3.98$, $Re = 6.79 \times 10^7$ m^{-1}, fin angle $\alpha = 16°$, $\delta_o = 3$ mm. In the similar computation of Panaras & Stanewsky (1992) the fin angle was also 16°, but the Mach number was 3.0 (milder interaction).

4.1. *Computational procedure*

The turbulence modelling procedure proposed by Panaras & Steger (1988) was applied in the present computation. Plots of the moment of vorticity profiles normal to the plate, at various crossflow stations are shown in figure 4. The plots correspond to the final solution. In these plots the index K of the grid in the direction normal to the plate is used as vertical coordinate. The numbers of the horizontal scale do not correspond to the actual values of the moment of vorticity, but are a multiple of it, in order to keep a constant horizontal spacing between the profiles. The three streamwise stations which are examined in figure 4 display the variation of the vorticity moment

in crossflow planes at the start of calculation (first set of curves, taken from right to left), in the middle of the computational field (second set of curves) and close to the outflow plane (third set of curves), respectively at $x = 3.0\delta_o$, $18.0\delta_o$ and $33.1\delta_o$. For each of these three stations, the moment of vorticity profiles at 6 or 8 crossflow positions have been drawn. The profiles cover the whole extent of the crossflow: the undisturbed boundary layer outboard of the separation (the first curve of each set, taken from right to left), the separation region (intermediate curves) and the reattachment region (one or two of the last curves).

Examination of any of the crossflow planes shown in figure 4 indicates that between the separation and the reattachment points the maximum of the moment of vorticity and its vertical position increase. Then in the reattachment region both these parameters decrease abruptly. Also, comparison of the three crossflow sections indicates that in the main flow direction the values of the maxima of the curves and their vertical positions are increased. This behaviour is expected, since in the downstream direction the separation vortex grows linearly (see figure 2). Finally, it is observed that at the second and third stations some of the curves in the separation domain have 3–5 maxima. Some of these maxima are caused by the shock formation and the shear layer which is formed at the triple-shock point (see figures 1*b* and 13*a*).

In each crossflow station of figure 4 a horizontal line has been drawn which approximately separates the overlying vortex structure from the surface boundary layer. It is observed that at the start of the interaction (right-hand station) the value of K_{cut} defined by the cut-off line is 51, then in the middle of the interaction it becomes equal to 56, and close to the end of the computational field equal to 59. If the suggestion of Panaras & Steger (1988) is followed, then in the whole flow field the mean value K_{cut}=56 has to be applied. In this case the calculated eddy-viscosity coefficients will be overestimated at the initial part of the interaction and they will be underestimated at the end of the computational field. Since the separation vortex in these types of flows grows linearly, instead of using a mean K_{cut} in the whole flow field, a linearly variable K_{cut} maybe assumed. Both these approaches were applied in the present calculations. It will be shown in the next section that the resulting predictions have very small differences and both agree very well with the experimental data.

4.2. *Comparison with the experiments*

Before starting to compare the results of the present calculations with the experimental data compiled by Settles & Dodson (1991), we present in figure 5 a perspective view of the pattern of the calculated skin-friction lines along with eight cross-sections of the vortices (visualized by the discriminant technique). Various elements of the structure of the flow about a sharp-fin/plate configuration, which were mentioned in § 2, are clearly shown in this figure. Visible on the plate is the remarkably rectilinear (away from the apex) separation line, as well as the reattachment one. Between them the secondary separation line is formed downstream of the third cross-section of the vortices. The core of the secondary vortex is gradually formed along the secondary separation line, between the core of the vorticity sheet and the primary vortex. Along the corner, the weak vortex detected for the first time by Kubota & Stollery (1982) grows.

Settles & Dodson (1991) give the plate pressure measured along a circular arc of radius $R = 101.6$ mm from the leading edge, versus the conical angle β. This angle is measured from the fin leading edge with respect to the free-stream direction. In the computational plate, we have found numerically which points of the mesh lie between the arcs $R - 0.5$ mm, $R + 0.5$ mm. Then the pressure at these points has

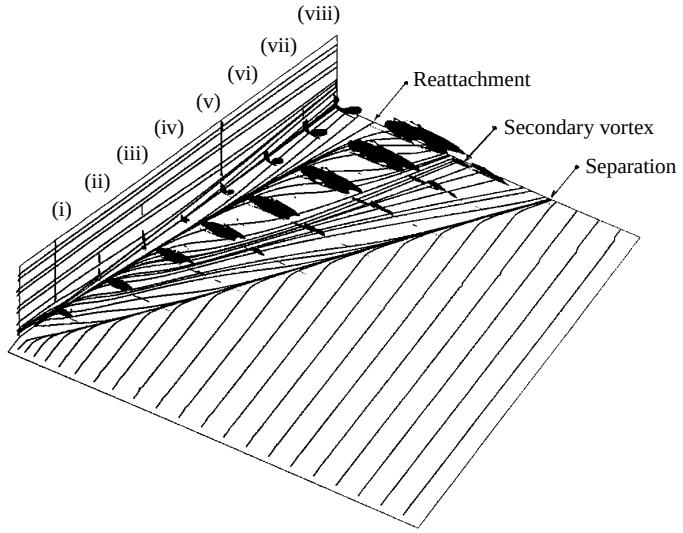

FIGURE 5. Pattern of skin-friction lines and cross-sections of the vortices.

been calculated. The experimental and the computed wall pressure distributions are compared in figure 6(*a*). Both solutions are shown, i.e. the one based on a constant K_{cut} along the whole flow field, and that based on the linear variable K_{cut}. For completeness, the solution found by application of the standard Baldwin–Lomax turbulence model is also included. The results which are based on the modified turbulence model agree very well with the experimental evidence. Over the whole extent of interaction there is coincidence of the predictions with the experimental data, with the exception of the reattachment region where the theoretical predictions provide higher values. On the other hand, the agreement of the solution which is based on the standard Baldwin–Lomax model is very poor. The spanwise extent is shorter, while the local minumum near $\beta = 27^\circ$ (which occurs under the core of the vortex) is not predicted well. There is agreement only on the level of the reattachment pressure.

The skin-friction comparison along the measurement arc ($R = 89$ mm) is shown in figure 6(*b*). Again the agreement of the theoretical predictions with the experiments is very good. Remarkable is the prediction of the secondary peak (at $\beta = 35^\circ$) close to which, according to Kim *et al.* (1991), the secondary vortex lies. This peak is not present in the solution which is based on the standard Baldwin–Lomax turbulence model, an indication that the secondary separation is not predicted. We note that in the reattachment region all our solutions predict a sharp peak. There are not enough experimental points in this region to verify this feature. However, in a picture of the oil-film interference-fringe pattern, which Kim *et al.* (1991) include in their paper, a strong fringe peak is clearly seen near the fin. According to these authors, the fringe pattern may be regarded as being qualitatively indicative of the actual skin-friction distribution.

Figure 6(*c*) shows the angles of the surface skin-friction lines, ϕ, plotted versus β along the measurement arc ($R = 89$ mm). The experimental points were extracted from pictures of the pattern of skin-friction lines. The local minimum at $\beta = 32^\circ$ corresponds to the secondary separation line. The agreement of the theoretical predictions is very good over the whole extent of the interaction. There is only a minor

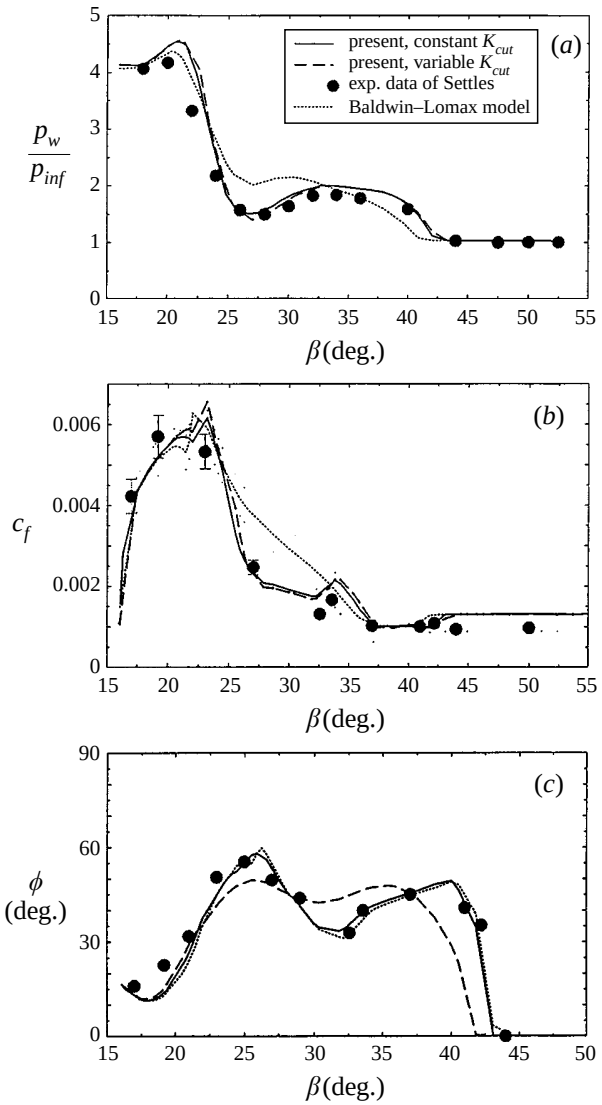

FIGURE 6. Comparison of calculated and measured data: (*a*) wall pressure; (*b*) skin friction; (*c*) flow angle at the wall.

disagreement close to the fin. The solution which is based on the standard Baldwin–Lomax turbulence model underpredicts the extent of interaction and the turning of the skin-friction lines in the region of secondary separation.

In figure 7 the experimental picture of the pattern of the skin-friction lines along the plate, obtained by using a kerosene-lampblack visualization technique, is compared with the theoretically calculated pattern of the skin-friction lines. Comparison of transparent versions of figures 7(*a*) and 7(*b*) has shown that the angles which the predicted separation lines (primary and secondary) form with the fin are equal to the experimental ones. In the case of the solution which is based on the standard Baldwin–Lomax turbulence model, the primary separation line forms a smaller angle

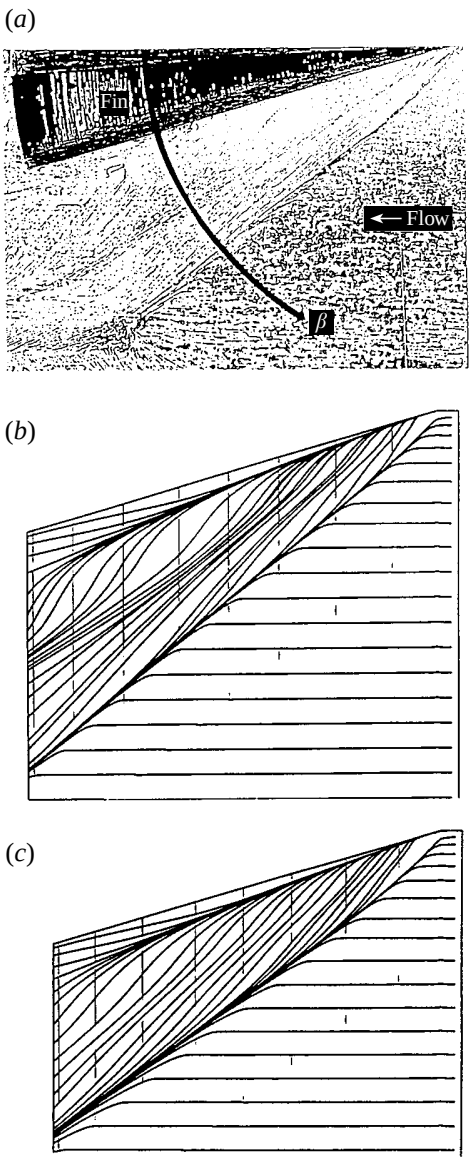

FIGURE 7. Surface flow pattern: (*a*) experimental; (*b*) calculated, K_{cut} turbulence model; (*c*) calculated, Baldwin–Lomax turbulence model.

with the fin, compared to the experimental picture, while no secondary separation line is formed.

5. Study of the structure of the conical vortex

The agreement of the calculated surface parameters (pressure, skin-friction distribution, etc.) with the experimental evidence suggests that the entire flow field is well simulated. Thus we may confidently proceed to post-processing of the numerical solution, in order to study the structure of the quasi-conical separation vortex in the context of turbulence modelling. Actually there is a fundamental difference between

the structure of a two-dimensional and a three-dimensional separation. In a closed two-dimensional separation, where a bubble is formed between the separation and the reattachment point, the outer part of the boundary layer, which has small intermittency, moves around the bubble without penetrating into it. However, the physics of a three-dimensional separation, like the one established about the configurations examined, is quite different. In this case the separation bubble is actually a vortex which attracts air from the outer layers, rotates it and guides some of it into the separation region. This process is evident in the flow model of Alvi & Settles (1992), shown in figure 1(*b*). But this model is schematic and not quantitative regarding the definition of the exact origin of the folded part of the boundary layer. This definition is critical, because possibly only the outer, low-intermittency, part of the undisturbed boundary layer penetrates into the separation bubble, resulting in the formation of a mixed type of bubble, partially turbulent and partially laminar.

To clarify this condition an analysis is done in which the flow field is represented by a number of stream surfaces, which originate within the upstream boundary layer and are initially parallel to the plate. Since the examined flow is steady, the stream surfaces will vary in space but not in time. By definition each of these surfaces is represented by a set of streamlines. The examined stream surfaces do not intersect, because initially they are parallel.

5.1. *Presentation of the flow field by stream surfaces*

In this section the spatial evolution of a selected number of stream surfaces which originate within the upstream boundary layer and initially are parallel to the plate is examined. Each of these surfaces is represented by a set of streamlines which originate from a corresponding set of grid points of the inflow plane. The distance of each set of grid points from the plate is constant. For the calculation of the streamlines the visualization system Comadi developed at DLR by Vollmers (1989) was used.

The spatial evolution of the first stream surface examined is shown in perspective view in figure 8(*a*). The streamlines of this surface initially lie extremely close to the plate ($y/\delta_o = 0.005$). It is observed that in this case almost all the streamlines which originate upstream of the region of separation are concentrated between the secondary vortex and the separation line. The majority of these deflected streamlines form the lifted-off vorticity sheet. The streamlines closest to the edge of the fin are entrained within the primary vortex. If the stream surface examined is located initially higher, at $y/\delta_o = 0.1$, many of its streamlines are entrained by the primary vortex and wind around its focus (figure 8*b*). With a further increase of the distance of the stream surface from the plate ($y/\delta_o = 0.3$), a larger part of the stream surface winds around the vortex focus, while its remaining lateral part is just lifted-off above the secondary vortex and the vorticity sheet (figure 8*c*). Observation of the trajectories of individual streamlines indicated that within the extent of the computational field they complete approximately one and a half turns.

The next stream surface examined, which is initially located at $y/\delta_o = 0.6$, behaves differently. The streamlines of this surface which lie upstream of the separation region do not wind around the focus of the vortex, but they fold over the core of the vortex, gradually enveloping the whole separation structure, from the rounded 'leading edge' of the vortex to the sharp 'trailing edge' of the vorticity sheet (figure 8*d*). The envelope formed has a remarkably conical shape, downstream of station (ii). Also, the penetration of the streamlines under the vortex start downstream of station (i). What is very important in this case is the fact that air which originates from a rather high layer of the boundary layer is guided underneath the vortex. The

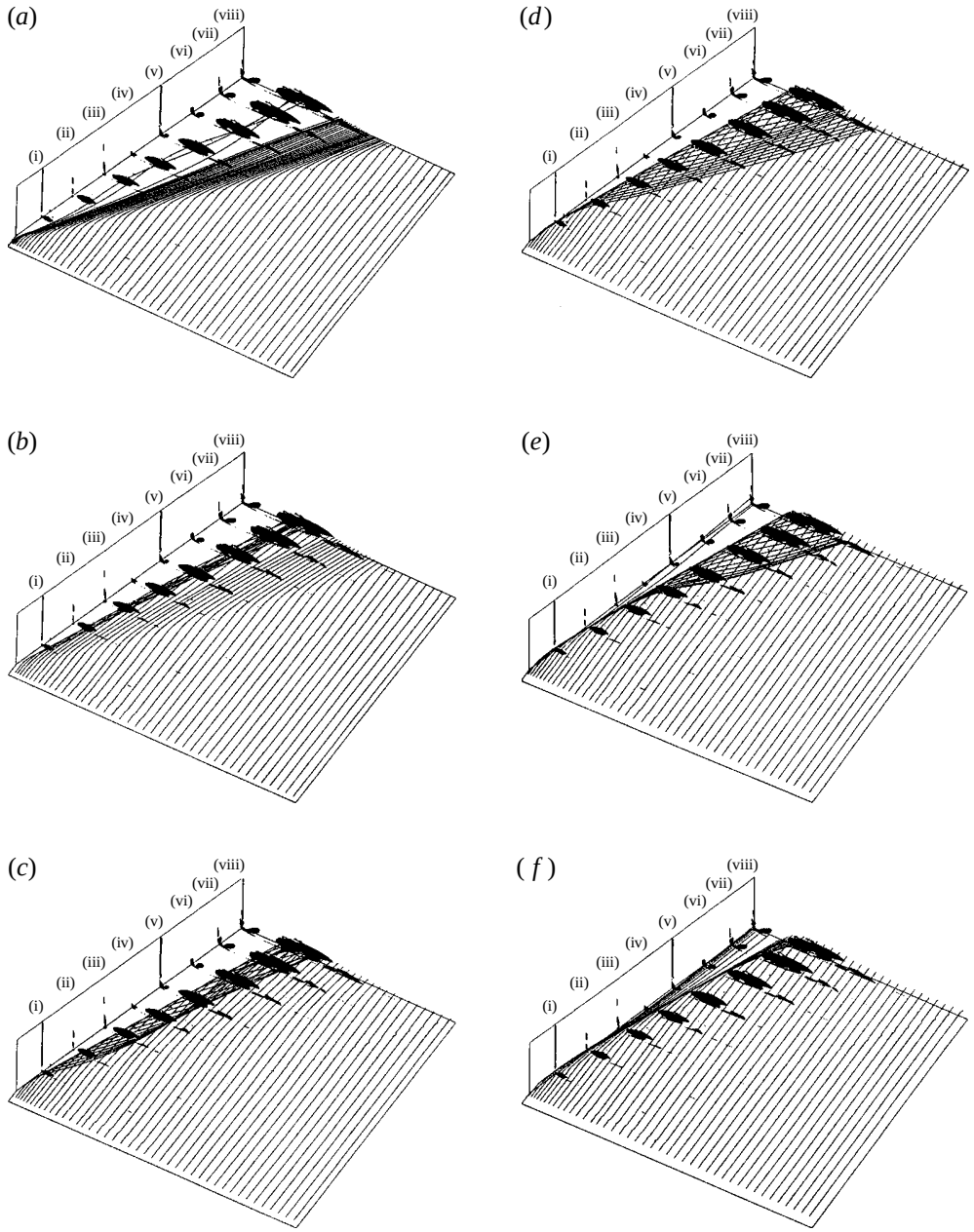

FIGURE 8. Development of stream surfaces originating at the inflow plate, at constant distance from the flat plate: (*a*) $y/\delta_o = 0.005$; (*b*) $y/\delta_o = 0.1$; (*c*) $y/\delta_o = 0.3$; (*d*) $y/\delta_o = 0.6$; (*e*) $y/\delta_o = 0.8$; (*f*) $y/\delta_o = 1.0$.

behaviour of the stream surface which is located at a height from the plate $y/\delta_o = 0.8$, is similar, i.e. its streamlines envelop the vortical structure (figure 8*e*). In this case, however, the penetration of the streamlines under the vortex starts later, downstream of station (iii). Also, the inward extent of the penetration is smaller. At the outflow plane the streamlines of this stream surface extend only from the leading edge of the primary vortex to the end of the secondary vortex.

The stream surface finally examined initially lies at the level of the boundary layer edge ($y/\delta_o = 1.0$). In this case, very few of the streamlines which lie ahead of the vortex fold around it. The majority of them fill the space between the fin and the vortex, or are lifted above the separation region. It is noteworthy that the streamlines which fill the space between the fin and the vortex come very close to the surface of the plate. This feature will be better demonstrated in cross-sections of the stream surfaces, which will be presented in what follows.

In summary, the preceding analysis revealed that the inner part of the undisturbed boundary layer winds around the focus of the conical separation vortex, forming the core of it, while the outer part just envelops the vortex without winding around it. The limiting stream surface seems to be the one which originates from the edge of the undisturbed boundary layer ($y/\delta_o = 1.0$), in the sense that air above it does not penetrate into the region underneath the vortex. Quantitative details of this process are given in figure 9, where the cuts of a number of stream surfaces through some crossflow planes are shown. Specifically, the crossflow planes (ii), (iv), (vi) and (viii) shown in figures 5 and 8 are used. In the resulting cuts (figure 9), the spiral motion of the inner part of the boundary layer (inner continuous lines), as well as the penetration of the outer layers under the vortex core are perfectly illustrated. In cross-section (ii), figure 9(*d*), the conical vortex is at its initial development phase. The outer part of the boundary layer ($y/\delta_o > 0.58$) envelops the vortex, but it does not penetrate into the region underneath it. Cross-section (iv), figure 9(*c*), lies at the middle of the computational field, and it is seen that the size of the vortex has been increased, while a considerable portion of the outer part of the boundary layer penetrates into the separation region. More particularly, the stream surface $y/\delta_o = 0.76$ folds under the core of the vortex. Further downstream, at sections (vi) and (viii), the $y/\delta_o = 0.76$ stream surface has formed an elongated region (tongue) underneath the vortex, which includes air that originates from the outer part of the boundary layer (between $y/\delta_o = 0.76$ and 1.0). The degree of lateral penetration of this tongue increases in the downstream direction. The similarity of the cross-section of the viscous layer shown in figure 9(*a*) with the physical flow-field model of Alvi & Settles (1991), figure 1(*b*), is evident. In both cases the secondary separation line has been detected below the tongue-like region. This issue will be examined in detail in the next subsection. The gradual thickening of the undisturbed part of the boundary layer (outboard of the separation region) is evident in figure 9.

The cross-sections of figure 9 also include the wall pressure distribution. The variation of the pressure is consistent with the development of the flow along the crossflow planes. As expected, a local minimum exists below the core of the vortex. This minimum decreases in the downstream direction. The maximum of the pressure appears at the reattachment region and it increases in the downstream direction. This behaviour reflects the mechanism of development of the conical vortex described previously, i.e. as the vortex develops in the flow direction, higher more energetic parts of the separated boundary layer impinge on the surface of the plate and penetrate into the separation region.

At this point recall that the flow at the outer region of a turbulent boundary layer is 'intermittent', which means that it alternates in time between being laminar or turbulent. According to the experiments of Klebanoff (1955), a boundary layer is intermittent from $y/\delta = 0.5$ to $y/\delta = 1.2$. How much of the time the flow is turbulent is defined by the intermittency factor, γ (equation (3.3)). Between the edge of the laminar sublayer and $y/\delta = 0.5$, where the flow is fully turbulent, the intermittency factor is $\gamma = 1.0$, while above $y/\delta = 1.2$ γ is zero (fully laminar flow). There is a

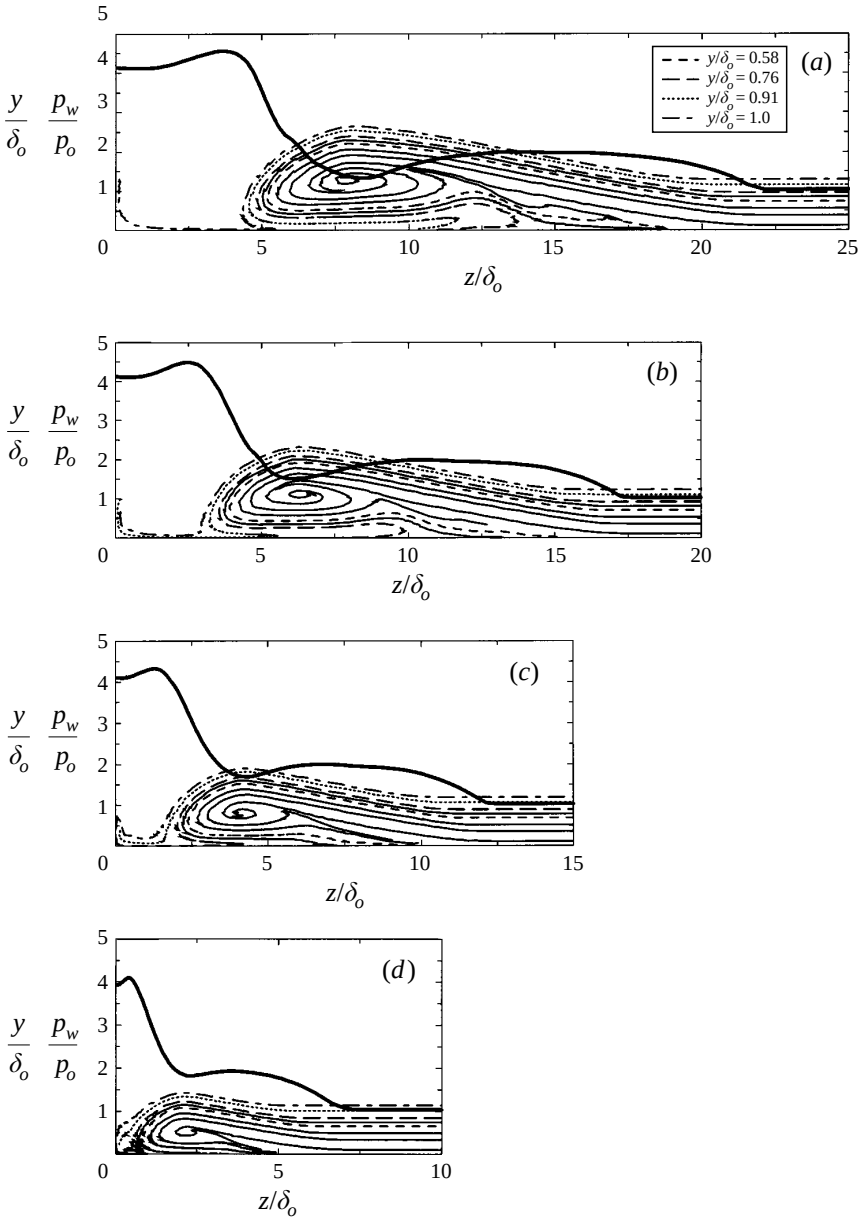

FIGURE 9. Cuts of the stream surfaces on crossflow planes, and wall pressure distribution (bold lines): (*a*) station (viii) of figure 5; (*b*) station (vi); (*c*) station (iv); (*d*) station (ii).

rapid fall in the value of the intermittency factor at the upper layers. For example, at $y/\delta = 0.8$ γ is 0.41, while at $y/\delta = 0.9$ its value is 0.19.

Interpretation of the data of figure 9, considering the intermittent character of the undisturbed boundary layer, leads to the conclusion that while the air which forms the spiral about the focus of the vortex is completely turbulent within the whole extent of the field, this does not happen in the case of the air which at the reattachment region penetrates into the separation region and envelops the core of the vortex. Since in the flow direction higher and higher layers fold over the core of

the vortex and penetrate into the separation region, gradually the turbulence level of the elongated penetration tongue, which is formed by these layers, is decreased. When the conical vortex starts to be formed close to the leading edge of the fin, it is completely turbulent. Gradually, as it grows in the downstream direction a low-turbulence tongue appears underneath it. This feature should be expected, because the conical vortex in its initial state of development is embedded within the turbulent part of the boundary layer and gradually emerges out of it as it grows in the downstream direction. On the contrary, according to the classical concept, which is based on observations of two-dimensional separations, the recirculatory region of a separation bubble is assumed to be always turbulent. This fundamental difference explains the tendency of most popular turbulence models, which are based on this classical concept, to underpredict strong swept-shock-wave/turbulent-boundary-layer interactions. In addition, considering the low-turbulence tongue as fully turbulent is the reason for the inability of the classical turbulence models to predict the secondary separation in the sharp-fin/plate flows investigated by Kim *et al.* (1991) and Knight *et al.* (1992).

5.2. *Secondary separation and low-turbulence tongue*

The core of the secondary vortex which appears in the flow examined has been visualized in figure 5 by the contours of the eigenvalues of the velocity gradient field. This vortex is very weak and is gradually formed between the secondary separation line and the core of the vorticity sheet. The technique of the stream surfaces which was used in the previous subsection for studying the structure of the reversed flow will be applied in what follows for the clarification of some features of the secondary vortex. As a first step, we observe in figure 5 that the secondary separation line, which actually is a set of closely spaced skin-friction lines, starts to be formed downstream of approximately the first 1/4 of the computational field (station (ii)). Initially it is curved, but gradually becomes straight and better defined. In the region of station (vi) a branching of the set of lines which constitute the secondary separation line is observed. The majority of the lines of the set turn slighly towards the fin, while some lines, which lie on the side of the primary separation line, start to diverge forming a weak reattachment line.

A synthesis of crossflow cuts and plate skin-friction lines is presented in figure 10. A large number of stream surfaces is used, covering not only the boundary layer, but also a part of the inviscid flow above it. The highest stream surface originates at $y/\delta_o = 1.95$. Starting the examination of the synthesis from station (viii), close to the outflow plane, it is observed in figure 10(*a*) that inboard of the core of the primary vortex the reversed part of the boundary layer expands and it is attracted towards the vortex. The lower stream surfaces are lifted-off the surface of the plate. At the region of reattachment of the lifted layer the upper stream surfaces continue to extend towards the separation region, where they reattach tangentially on the plate, or interact with the flat vorticity sheet which extends upwards from the primary separation point. On the other hand, the lower stream surfaces turn around and reattach under the core of the primary vortex. It is remarkable that there is a concentration, or rather a convergence, of turned-around stream surfaces above the region of the set of secondary separation lines. The resulting flow structure is a typical secondary separation vortex. However, in the visualization technique used here a vortex should exhibit a spiral core. The non-existence of such a core means that the particular secondary vortex is very weak. Examining the trajectories of streamlines which pass through this vortex we found that within the extent of the computational

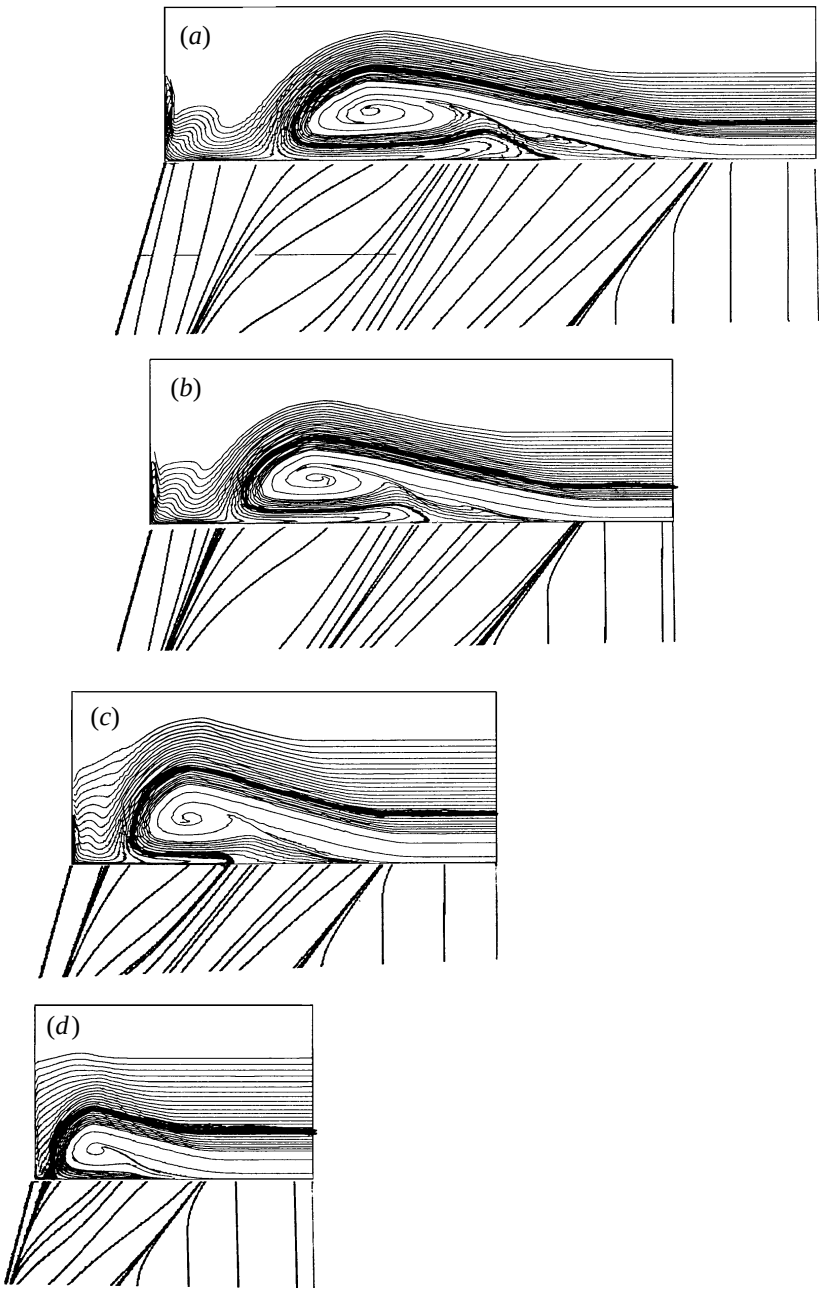

FIGURE 10. Synthesis of cuts of stream surfaces and of skin-friction lines: (*a*) station (viii) of figure 5; (*b*) station (vi); (*c*) station (iv); (*d*) station (ii). The bold lines are for $y/\delta_0 = 0.71$.

field it is hard to detect, optically, any rotation. On the other hand, as we have mentioned already, some of the streamlines that wind around the core of the primary vortex complete more than one turn within the computational field. Also very weak is the longitudinal vortex which is formed at the corner. At this point recall that both these vortices are detected in the contours of the eigenvalues of the velocity gradient field (figure 5).

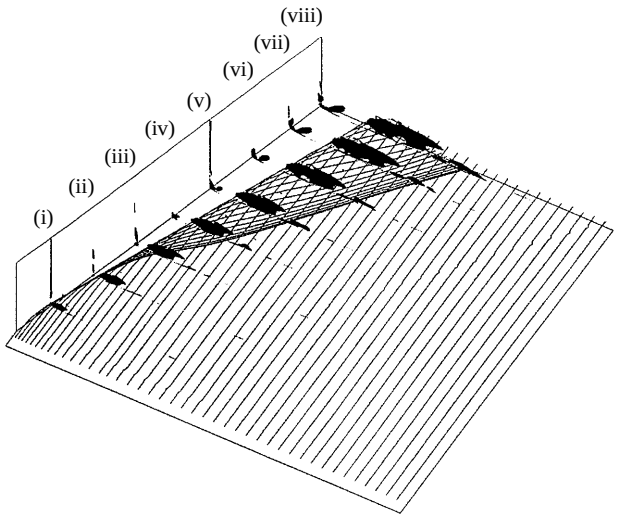

FIGURE 11. Development of the stream surface which originates at $y/\delta_o = 0.71$.

The conditions are similar in the case of the cross-section (vi), figure 10(*b*). The secondary separation vortex is formed, but it is smaller and weaker (its lifting is smaller). Also, fewer turned-around stream surfaces terminate at the plate in the region of the secondary separation line. Further upstream, at station (iv), there is no visible lifting of the lower part of the reversed flow inward of the core of the primary vortex. Also, the major splitting of the boundary layer occurs at the reattachment region of the primary vortex. Very few stream surfaces turn around in the region of the secondary separation. In addition we note that at this station the discriminant of the velocity gradient tensor does not detect any vorticity concentration above the secondary separation line (see figure 5). It seems that at station (iv) a small 'bump' has started to be formed, which leads to the appearance of the secondary separation line. Finally, at station (ii), which is upstream of all the other sections shown in figure 10, the whole reversed part of the boundary layer flows towards the separation point. There is splitting of the boundary layer only in the region of reattachment. Also, there is no indication of a secondary separation line on the surface of the plate.

In the cross-sections which are shown in figure 10 the cut of the stream surface which starts at $y/\delta_o = 0.71$ has been denoted by a bold line. This line bounds the secondary separation vortex in the cross-sections (vi) and (viii) where this vortex is developed, while in section (iv), where the secondary vortex is in an incipient state, the bold line terminates at the secondary separation line. Further upstream, in section (ii), where there is no secondary vortex, the $y/\delta_o = 0.71$ stream surface and the layers above it do not penetrate into the separation region, but at the reattachment region of the primary vortex they turn towards the fin. This observation leads to the conclusion that the secondary vortex is composed by air which originates in the outer part of the boundary layer, which is characterized by low turbulence. Actually, the secondary separation vortex forms the tip of the low-turbulence tongue. In the perspective view of figure 11 it is clearly shown that the reversed part of the stream surface $y/\delta_o = 0.71$ extends laterally under the vortex beyond or, at least till, the region of appearance of the secondary separation vortex. This figure indicates that in the flow examined the secondary separation appears somewhere between station (iv) and (v).

For an appreciation of the effect of the higher eddy-viscosity values predicted

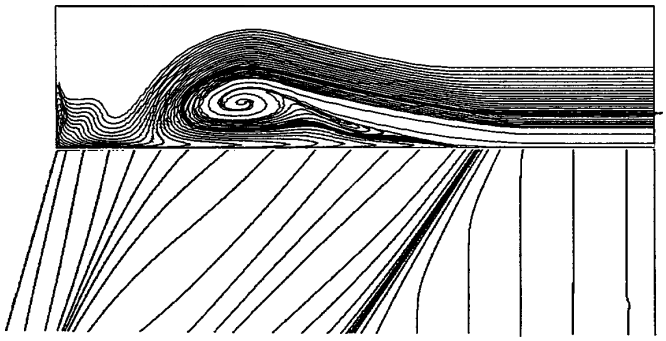

FIGURE 12. Flow field of solution based on the Baldwin–Lomax turbulence model.

by the standard Baldwin–Lomax model on the overall development of the flow, a synthesis of the related simulation is shown in figure 12, similar to that shown in figure 10(*a*). Comparison of figures 10(*a*) and 12 indicates that the flow simulation which is based on the standard Baldwin–Lomax model is qualitatively similar to that predicted by the K_{cut} model. In this simulation also, the higher, low-turbulence, part of the boundary layer folds under the primary vortex. However, since in this case the secondary separation vortex is not predicted, the low-turbulence region looks rather like a wedge and not like a tongue. In addition, it is observed in figure 12 that in this solution also, the reverse flow is lifted inward of the primary vortex core. However, only the layers which are close to the vortex core are lifted-off. The stream surfaces which are close to the plate are not lifted at all, though some of them turn around at their reattachment region. But the turned-around stream surfaces do not converge to create the close set of the secondary separation lines, instead they are almost evenly spaced. On the surface of the plate, the skin-friction pattern is consistent with the features of the overlying flow. Within the separation region the skin-friction lines extend from the reattachment line towards the separation one. There is no secondary separation line. This behaviour can be explained by the fact that the turbulence level of the Baldwin–Lomax solution in the region of the low-turbulence tongue is high, compared to that of the K_{cut} solution (see the next subsection).

5.3. *Explanation of the success of the K_{cut} turbulence model*

In this subsection it will be shown that the remarkable success of the calculations in which the vortex is excluded from the estimation of the eddy-viscosity coefficients (modified Baldwin–Lomax model) is due to the fact that this model predicts very small values of the eddy-viscosity coefficients in the region of the low-turbulence tongue.

To compare the modified with the standard Baldwin–Lomax turbulence model, in figure 13(*a*) are shown some profiles of the moment of vorticity along the crossflow plane (vi) of figure 5 (streamwise position $x = 28.1\,\delta_o$). In this case, the physical distance from the wall is used as vertical coordinate. It is seen that these profiles provide a good visualization of the shape and size of the cross-section of the separation vortex, as well as of the shock formation, including the curved shear layer which is formed at the shock triple point and moves towards the corner (see also the flow-field model of Alvi & Settles 1992, shown in figure 1*b*). The short-dashed line in figure 13(*a*) connects the points of maximum value of the moment of vorticity, which are used in the standard Baldwin–Lomax model. The long-dashed line connects the points where the moment of vorticity becomes maximum, under the restriction of

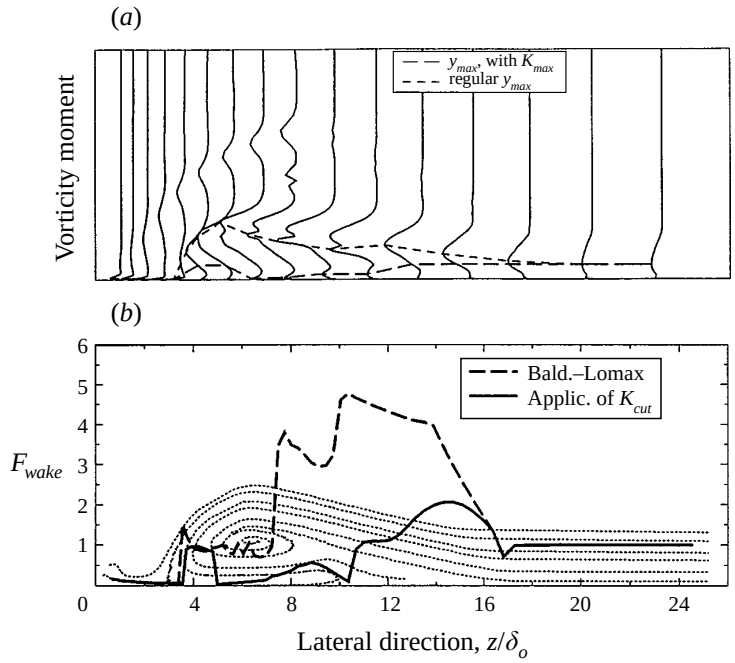

FIGURE 13. Comparison of turbulence parameters at station (vi): (*a*) y_{max}; (*b*) F_{wake}.

terminating the search at K_{cut} (exclusion of the vortex from the calculation of the eddy-viscosity coefficients, see § 4.1). Comparison of these two curves indicates that in the separation region the distance normal to the wall, η_{max}, which is predicted if the vortex is excluded from the calculation of the maximum values of the moment of vorticity, is much smaller than the one assumed by the standard Baldwin–Lomax turbulence model. The values of η_{max} become particularly small in the region of the low-turbulence tongue. Below the core of the vortex these values become almost zero, indicating that large gradients of the velocity exist close to the wall.

Since, according to equation (3.2), the eddy viscosity is proportional to the function F_{wake}, it is sufficient to use this function in the comparison of the two versions of the Baldwin–Lomax turbulence model. This is done in figure 13(*b*), where the variation of the function F_{wake} along the (vi) crossflow plane is shown. The values of F_{wake} have been non-dimensionalized by its value at the region where the flow is attached. It is observed that the two versions of the Baldwin–Lomax model provide similar values for the function F_{wake} in the regions of separation and reattachment points, but the values between these points are much smaller in the case of the modified model. The values are particularly small in the region of the low-turbulence tongue. In some points the predicted values are almost zero (laminar flow). In the region of the secondary vortex the wake function predicted by the modified model is approximately equal to one sixth of that predicted by the standard Baldwin–Lomax model. This observation supports the view that the success of the modified turbulence model is due to the appropriate modelling of the flow in the region of the low-turbulence tongue.

The F_{wake} functions of the two versions of the Baldwin–Lomax turbulence model are compared in figure 14 at station (ii), where the low-turbulence tongue has not been developed yet. It is seen that in this station the two predictions are closer. Small

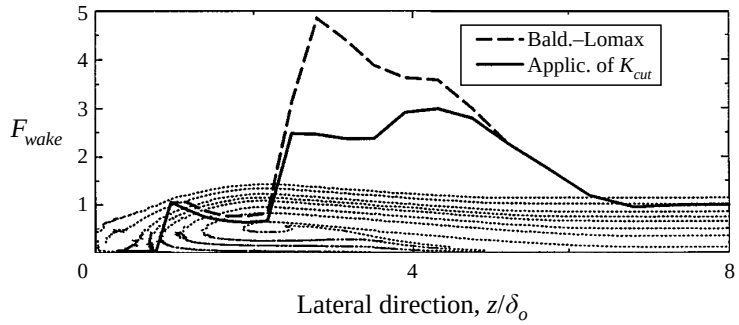

FIGURE 14. Comparison of F_{wake} at station (ii).

differences exist only between the separation point and the core of the primary vortex. Between the core of the vortex and the reattachment region the two predictions are almost identical. This behaviour of the K_{cut} model is explained by the fact that because of the non-existence of the low-turbulence tongue, there are no large gradients of the velocity close to the surface of the plate. Thus, the maximum values of the profiles of the moment of vorticity appear not close to the plate, as it happens in station (vi), but higher, close to the prediction of the Baldwin–Lomax model. In practice it means that the K_{cut} model predicts small values of the eddy-viscosity coefficient only where almost laminar flow exists underneath the vortex core. In the initial part of the conical separated flow, where the air in the reversed flow is turbulent, the eddy-viscosity coefficient takes high values.

In summary, the data presented in this section indicate that the major feature of the turbulence model which is based on the concept of Degani & Schiff (1986) is the prediction of very small eddy-viscosity values between the core of the vortex and the reattachment. Since within this region a low-turbulence tongue exists, it appears that the modified turbulence model simulates efficiently the surface flow. However there is an adverse side effect on the modelling of the core of the overlying vortex, which though it consists of the turbulent part of the undisturbed boundary layer, it is simulated as almost laminar. This leads to the conclusion that the Degani–Schiff modification improves the accuracy of prediction of the surface layer, but not of the outer part of the flow field. Conceptually this is true and there is no way to correct this condition, which occurs because the functional form of the equations which are used in the algebraic turbulence models follows the structure of a boundary layer: the existence of turbulent air above the surface layer is excluded. However, since the trace on the surface of the plate of the development of the linearly growing vortex is accurately predicted, the same will happen in the normal direction. Actually the core of the turbulent vortex occupies only a small portion of the quasi-conical interaction domain.

6. Discussion, concluding remarks

In § 5.1, calculation of the spatial evolution of some selected stream surfaces of the main test-case flow has revealed that the quasi-conical vortex, which appears in strong swept-shock/turbulent-boundary-layer interactions, initially is composed exclusively of turbulent air. But as the vortex grows in the downstream direction, only its core continues to be composed of turbulent air, while under the vortex, along the surface of the plate, gradually a low-turbulence tongue is formed. This happens because the

outer part of the boundary layer, which is composed of low-turbulence air, rotates around the vortex and at the reattachment region penetrates into the separation bubble. In addition it has been found that within the extent of the computational field the $y/\delta_o = 1.0$ surface envelops the conical separation air, without penetrating it at the reattachment region. However, it is anticipated that further downstream higher layers, of purely inviscid air, are entrained within the tongue.

The intermittency of the air which constitutes the tongue formed under the vortex is very small. The present analysis is not appropriate for the derivation of particular numbers. This issue can be resolved only by experiments, which we hope will follow. At this point we can only mention that in the examined $M_\infty = 4.0$, $\alpha = 16^\circ$ flow, if the intermittency-factor curve of Klebanoff is assumed to be valid for compressible flows, then the layers which constitute the low-turbulence tongue initially, i.e. before passing through the shock system, have intermittency factor between 0.5 and 0. The interaction of these layers with the vorticity of the shock waves, as well as the deceleration at the region of folding around the 'leading edge' of the primary vortex, are destabilizing factors. Thus, the turbulence level of the tongue will be a little higher than that of the layers which form it. If the fin is very long, then a transition to turbulence may occur. In this case, the part of the reversed flow which is closer to the primary separation line will be affected, because the air of this part travels the longest distance under the vortex (see figure 11). However, at the same time that the 'older' part of the reversed flow becomes turbulent, new low-turbulence air will be entrained into the root of the tongue, at the reattachment region of the vortex.

As regards the secondary separation vortex, which appears in strong shock-wave/turbulent-boundary-layer interactions, it has been found that in the test case it forms the tip of the low-turbulence tongue. This vortex starts to be formed at a streamwise position at which the penetrating tongue reaches the expansion region which exists between the core of the primary vortex and the primary separation line. The formation of the secondary separation line on the surface of the plate is an early indication that a 'bump' starts to be formed. Further downstream, as the low-turbulence tongue penetrates more into the separation region, the core of this vortex is formed and finally the secondary reattachment line appears on the plate. In the test case the secondary vortex is very weak. No spiral motion within the extent of the computational field has been detected.

For investigating the effect of the strength of the interaction on the structure of the reversed flow, we have calculated some additional sharp-fin/plate test cases from the data-base of Settles & Dodson (1991). Comparisons of some of these additional cases with experiments are included in a follow-up paper (Panaras 1997), in the context of a new turbulence model. Crossflow cuts of the additional flows, as well as of the main test-case are shown in figure 15. The cuts correspond to station (viii) and they have been arranged according to the interaction strength. The first cut belongs to a weak interaction, $M_\infty = 3.0$, $\alpha = 10^\circ$. It is seen in figure 15(*a*) that qualitatively this flow develops as described previously. Thus, a primary vortex is formed, around which a part of the separated boundary layer folds and penetrates into the separation region. However, the vortex is very weak (the spiral core is small), and the folded layer originates from the inner part of the boundary layer and not from the outer one. Hence, there is no formation of a low-turbulence tongue. Observation of the surface skin-friction lines (not included here) has indicated that no secondary vortex appears (this is also evident in the data of Alvi & Settles 1992).

A stronger interaction is shown in figure 15(*b*), where the Mach number is still equal to 3.0 but the angle of the fin is 16°. This flow case has been studied earlier

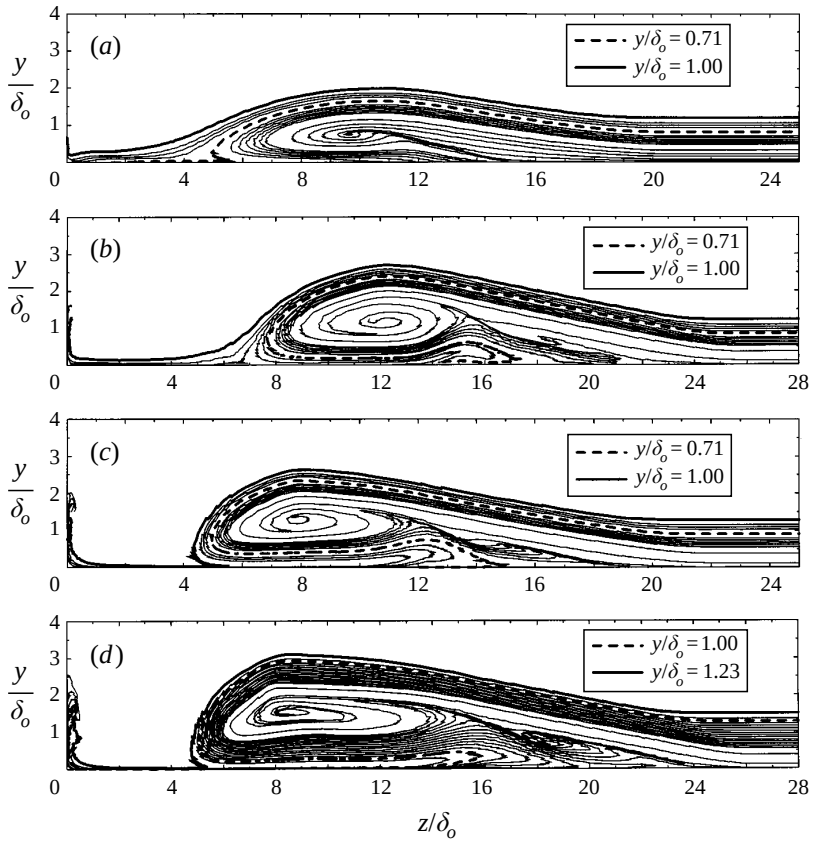

FIGURE 15. Cross-sections of various flows: (*a*) $M_\infty = 3.0$, $\alpha = 10°$; (*b*) $M_\infty = 3.0$, $\alpha = 16°$; (*c*) $M_\infty = 4.0$, $\alpha = 16°$; (*d*) $M_\infty = 4.0$, $\alpha = 20°$.

by Panaras & Stanewsky (1992). It is seen in figure 15(*b*) that the structure of this flow is very similar to that of the main test case (shown in figure 15*c*). The low-turbulence tongue is formed and its tip has the characteristic shape that denotes the existence of a secondary vortex. Also, the $y/\delta_o = 0.71$ stream surface envelops the secondary vortex. There is only one difference from the stronger main test case: at the reattachment region the stream surface $y/\delta_o = 1.0$ and some lower ones do not fold around the vortex, but they extend towards the fin. This means that the intermittency of the low-turbulence tongue of this flow is smaller that that of the main test case. However, at the other extreme is the flow examined in figure 15(*d*). This interaction is generated in a $M_\infty = 4.0$ and $\alpha = 20°$ fin/plate flow, and the stream surface $y/\delta_o = 1.0$ penetrates deeply into the separation region and it is, actually, a part of the secondary vortex. Furthermore, the layers of the tongue adjacent to the plate (under the primary vortex) are practically laminar, because they are composed of air which originates outside the boundary layer (between $y/\delta_o = 1.0$ and 1.23). Remarkable is the fact that in this strong interaction the penetration of the $y/\delta_o = 1.0$ stream surface into the separation region starts in the middle of the computational field (figure 16).

In summary, the data of figure 15 indicate that the turbulence level of the elongated tongue which is formed under the core of the vortex depends on the strength of the interaction. Increase of the interaction strength results in reduction of the turbulence level of the tongue. The existence of this low-turbulence tongue in strong swept-

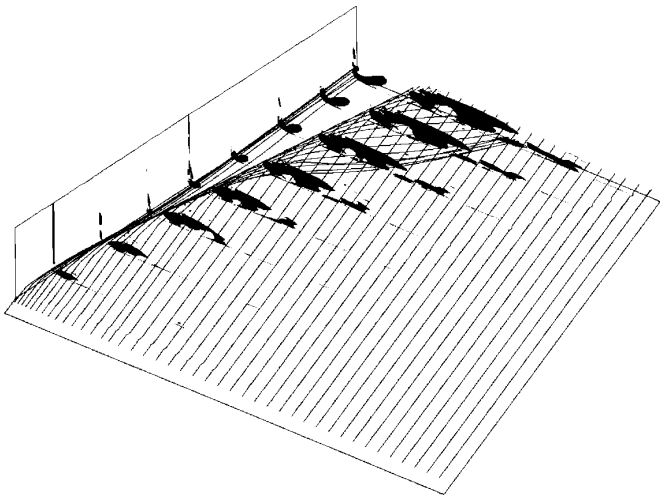

FIGURE 16. Development of the stream surface which originates at $y/\delta_o = 1.0$, flow conditions: $M_\infty = 4.0$, $\alpha = 20°$.

shock-wave/turbulent-boundary-layer interactions creates a mixed-type separation bubble: turbulent in the region of the separation line and almost laminar between the reattachment line and the secondary vortex. This type of separation is not possible to simulate accurately with the currently existing algebraic turbulence models, because the eddy-viscosity relations of these models are based on the physics of two-dimensional flows, where in a separation bubble the whole recirculation region is turbulent. A proof of this statement was given in § 5.3, where it was demonstrated that the modified Baldwin–Lomax turbulence model, which simulated very successfully the sharp-fin/plate flows examined, predicts very small values of the eddy-viscosity coefficients in the region of the low-turbulence tongue, compared to the values predicted by the regular Baldwin–Lomax model. As regards the failure of the $k-\epsilon$ model to predict accurately the sharp-fin/plate flows examined by Knight *et al.* (1987) and by Kim *et al.* (1991), most probably it is also due to poor simulation of the low-turbulence tongue. This view is based on the fact that in this model the production terms depend on the derivatives of the mean velocity vector, while large variations of the velocity are observed within the low-turbulence tongue (see figure 13*a*). To clarify this issue, a detailed study of the variation of the eddy-viscosity coefficient given by the $k-\epsilon$ model within the separation region is necessary, requiring large-scale calculations employing this model.

This discussion leads to the conclusion that for improving the reliability of the existing algebraic turbulence models in predicting strong swept-shock-wave/turbulent-boundary-layer interactions, it is necessary to develop new equations for the calculation of the eddy viscosity in the separation region, which will consider the existence of the low-turbulence tongue. The present author (Panaras 1997) has developed such a model, based on the Baldwin–Lomax formulation and simulating accurately various sharp-fin/plate test cases. This model indirectly verifies the existence of the low-turbulence tongue.

Finally, it is quite probable that low-turbulence air also exists underneath the core of the vortices in other types of turbulent flows which are characterized by the appearance of extensive crossflow separation. Typical examples are the high-incidence flows about delta wings and slender bodies.The methodology followed in the present

analysis should be applied in these types of flows for investigating the exact structure of the separation vortices.

This work was done while the author was visiting scientist at DLR, as recipient of a research fellowship awarded by the European Union, within the Human Capital and Mobility programme. The assistance of the European Union is acknowledged, as well as that of DLR, which provided the computational means and all the required support. The author wishes to thank Dr W. Kordulla for his invitation to work in the Numerical Department of the Institute of Fluid Mechanics, and Dr D. Schwamborn for the hospitality and the fruitful discussions regarding turbulence modelling.

REFERENCES

Alvi, F. S. & Settles, G. S, 1992 Physical model of the swept shock/boundary-layer interaction flowfield. *AIAA J.* **30**, 2252–2258.

Baldwin, B. S. & Lomax, H. 1978 Thin layer approximation and algebraic model for separated turbulent flows. *AIAA Paper* 78-257.

Cebeci, T. & Smith, A. 1974 *Analysis of Turbulent Boundary Layers*. Academic.

Degani, D. & Schiff, L. B. 1986 Computation of turbulent supersonic flows around pointed bodies having crossflow separation. *J. Comput. Phys.* **66**, 173–196.

Degani, D., Schiff, L. B. & Levy Y. 1991 Numerical prediction of subsonic turbulent flows over slender bodies at high incidence. *AIAA J.* **29**, 2054–2061.

Gerhold, T. & Krogmann, P. 1993 Investigation of the hypersonic turbulent flow past a blunt fin/wedge configuration. *AIAA Paper* 93-5026.

Hung, C. M. & MacCormack, R. W. 1978 Numerical solution of three-dimensional shock wave and turbulent boundary-layer interaction. *AIAA J.* **16**, 1090–1096.

Kim, K. S., Lee, Y., Alvi, F. S., Settles, G. S. & Horstman, C. C. 1991 Laser skin friction measurements and CFD comparison of weak-to-strong swept shock/boundary layer interaction. *AIAA J.* **29**, 1643–1950.

Klebanoff, P. S. 1955 Characteristics of turbulence in a boundary layer with zero pressure gradient. *NACA Rep.* 1247.

Knight, D. D. 1993 Numerical simulation of 3-D shock wave turbulent boundary layer interaction. *AGARD-R*-792, paper No. 3.

Knight, D. D., Badekas, D., Horstman, C. C., Shapey, B. & Settles, G. S. 1992 Quasiconical flowfield structure of the three-dimensional sharp fin interaction. *AIAA J.* **30**, 2809–2816.

Knight, D. D., Horstman, C. C., Shapey B. & Bogdonoff, S. 1987 Structure of supersonic turbulent flow past a sharp fin. *AIAA J.* **25**, 1331–1337.

Kubota, H. & Stollery J. L. 1982 An experimental study of the interaction between a glancing shock wave and a turbulent boundary layer. *J. Fluid Mech.* **116**, 431–458.

Panaras, A. G. 1992 Numerical investigation of the high-speed conical flow past a sharp fin. *J. Fluid Mech.* **236**, 607–633.

Panaras, A. G. 1996 Review of the physics of swept-shock/boundary-layer interactions. *Prog. Aerospace Sci.* **32**, 173–244.

Panaras, A. G. 1997 Algebraic turbulence modelling for swept shock-wave/turbulent boundary-layer interactions. *AIAA J.* to appear.

Panaras, A. G. & Stanewsky, E. 1992 Numerical study of secondary separation in glancing shock/turbulent boundary layer interactions. *AIAA Paper* 92-3666.

Panaras, A. G. & Steger J. L. 1988 A thin-layer Navier–Stokes solution of the flow about a prolate spheroid. *Z. Flugwiss.* **12**, 173–180.

Roe, P. L. 1981 Approximate Riemann solvers, parameters vectors and difference schemes. *J. Comput. Phys.* **43**, 357–372.

Settles, G. S. 1993 Swept shock/boundary-layer interactions-Scaling laws, flowfield structure, and experimental methods. *AGARD-R*-792, paper No. 1.

Settles, G. S. & Dodson, L. J. 1991 Hypersonic shock/boundary-layer interaction database. *NASA CR*-117577.

Token, K. H. 1974 Heat transfer due to shock wave/turbulent boundary layer interactions on high speed weapon systems. *AFFDL TR*-74-77.

Vollmers, H. 1989 A concise introduction to Comadi. *DLR IB* 221-89 A 22.

Vollmers, H., Kreplin, H. P. & Meier, H. U. 1983 Aerodynamics of vortical type flows in three dimensions. *AGARD C. P.* 342, paper 14.

Yee, H. C. & Harten, A. 1987 Implicit TVD schemes for hyperbolic conservation laws in curvilinear coordinates. *AIAA J.* **25**, 266–274.